Simulation of J-aggregate microcavity photoluminescence

Paolo Michetti*
Dipartimento di Fisica, Università di Pisa, Largo Bruno Pontecorvo 3, 56127 Pisa, Italy

Giuseppe C. La Rocca†
Scuola Normale Superiore and CNISM, Piazza dei Cavalieri 7, 56126 Pisa, Italy

(Received 24 September 2007; revised manuscript received 25 January 2008; published 1 May 2008)

We have developed a model in order to account for the photoexcitation dynamics of J-aggregate films and strongly coupled J-aggregate microcavities. The J aggregates are described as a disordered Frenkel exciton system in which relaxation occurs due to the presence of a thermal bath of molecular vibrations. The correspondence between the photophysics in J-aggregate films and that in J-aggregate microcavities is obtained by introducing a model polariton wave function mixing cavity photon modes and J-aggregate super-radiant excitons. With the same description of the material properties, we have calculated both absorption and luminescence spectra for the J-aggregate film and the photoluminescence of strongly coupled organic microcavities. The model is able to account for the fast relaxation dynamics in organic microcavities following nonresonant pumping and explains the temperature dependence of the ratio between the upper polariton and the lower polariton luminescence.

DOI: 10.1103/PhysRevB.77.195301 PACS number(s): 78.66.Qn, 71.36.+c, 78.20.Bh, 71.35.Aa

I. INTRODUCTION

Strongly coupled microcavities (MCs) are structures that confine light in the vertical direction around an optically resonant layer: when the light-matter interaction is larger than the damping processes, the system eigenstates are a coherent superposition of the confined photon modes and the two-dimensional (2D) excitons, which are the cavity polaritons. Their dispersion relation is characterized by the presence of the upper polariton (UP) and lower polariton (LP) branches separated at the anticrossing by the Rabi splitting.

Inorganic semiconductor MCs typically employ one or more quantum wells as the active layer. In such structures grown by molecular beam epitaxy, 2D Wannier excitons and photons couple conserving the in-plane wave vector as a good quantum number. Since the pioneering work by Weisbuch *et al.*,[1] the physics of semiconductor strongly coupled MCs had been analyzed in great detail.[2–6] For low pumping intensities, the dynamics of QW microcavities is characterized by the occurrence of the bottleneck effect,[7] which results from the competition of small polariton radiative lifetime with the relaxation induced by scattering with acoustical phonons. The relaxation bottleneck can be overcome at higher pumping intensities, thanks to the bosonic behavior of polaritons, which show stimulated scattering at a sufficiently high population density with the signature of a threshold behavior.[8–10] The increase in the MC quality factor and the search for optically active materials capable of a greater Rabi splitting (tens of meV) have led to the recent success of observing polariton condensation[11] from nonresonant pumping.

On the other hand, strongly coupled organic microcavities had been developed since 1998 (Ref. 12) by using different kinds of optically active organic layers. The spin-coated cyanine dye J-aggregate films are probably the most typical, but materials with observable vibronic replicas have also been used.[13,14] For a detailed review on organic MCs, see Refs. 15–20. The main advantages of organic based microcavities are the simplicity of construction and the huge possibilities of choosing optically active molecules *ad hoc*. Most importantly, organic MCs allow obtaining greater values of the Rabi splitting[21] (typically 100–200 meV) with respect to inorganic semiconductor microcavities and offer the possibility of easily observing polaritons at room temperature.[22]

In J aggregates, the molecular Frenkel excitons have an energy dispersion curve, which is the J band, due to the excitation transfer interaction, and most of the oscillator strength are concentrated on the so-called super-radiant excitons at the bottom of the band. In J-aggregate microcavities, the polaritons are the result of the strong light-matter interaction between such super-radiant excitons localized on each aggregate and the photon cavity modes extended over the whole structure. The nature of polaritons in organic microcavities based on disordered J-aggregate films had been theoretically studied through analytical[23,24] and numerical[25–27] approaches. In particular, the coexistence of delocalized cavity polaritons with a well defined wave vector and localized incoherent excitations has been proven. Thus, the excitation spectrum of such a microcavity is composed, besides the polariton branches, of a huge reservoir of molecular excitons that are not strongly coupled. The efforts to understand the dynamics of organic MC polaritons focused on the photoluminescence intensity ratio between UP and LP photoluminescence as a characteristic signature of the relaxation processes in organic MCs.[19,28,29] The relaxation model proposed in Ref. 28 was based on the idea that polaritons are pumped by radiative decay of the reservoir excitons (proportional to the bare film photoluminescence) and that the competition of nonradiative interbranch scattering against the polariton time of escape through the mirrors determines the emission intensity ratio between the branches. In such a scenario, a particular role is attributed to a specific vibrational mode resonant with the Rabi splitting. Later on,[23,30,31] the possibility of nonradiative scattering from the exciton reservoir (ER) to the polaritons through the interaction with molecular vibrations was introduced and theoretically investi-

gated as an effective process in determining the polariton relaxation and steady state population following nonresonant optical pumping. Still, a full numerical model of the complex MC dynamics scenario, taking into account the aggregate J-band excitons (and not only the super-radiant ones) and all of the possible relaxation channels, is missing until now.

The nature of the optical properties of molecular aggregates had been debated for a long time.[32] A typical example of such materials are the J aggregates of the dye pseudoisocyanine[33–35] (PIC) and in order to explain their optical features, different interpretations have been suggested based on activated processes involving optical or acoustic phonons of the aggregate,[34] host vibrations,[35] and exciton self-trapping phenomena.[36] Recently, J-aggregate dynamics has been modeled as a disordered Frenkel exciton system in which relaxation happens by means of scattering with a continuous spectrum of local vibrations and studied by means of a Pauli master equation approach.[37] This approach was successful in explaining the interplay of disordered local structures of the aggregates and relaxation dynamics leading to the nonmonotonous behavior of the Stokes shift[38] and PIC aggregate thermal line broadening.[39]

In the present work, we base our description of the photophysics of a J-aggregate film to be used as the optically active layer of J-aggregate microcavities on the latter approach. Then, we turn on the strong light-matter interaction and generalize our model to treat the formation of exciton polaritons. Also, in the strong coupling regime, the Frenkel exciton component of the MC excitations suffers the same relaxation mechanisms as those for the J-aggregate film in noncavity samples, interacting with the same thermal bath of vibrations. Our aim is to develop a generic model to see how far the approach successfully employed for the description of J-aggregates films[37–39] can go in describing the physics of such films embedded in a strongly coupled microcavity without introducing any further parameter. We should remark that in this spirit, we do not consider the possible presence of a specific optical vibrational mode resonant with the upper to lower polariton splitting. Of course, such a mode can be important and in order to obtain a full description of all details of the MC photoluminescence dynamics, a precise knowledge of its specific vibrational spectrum would be needed.

We apply our model to simulate the MC photoluminescence following nonresonant pumping. The scattering due to the vibrational bath determines the relaxation of initially high energy molecular excitations toward the states at the bottom of the J band and eventually toward the exciton polaritons. The photonic part of the mixed excitations determines their escape rate through the mirrors, which is the radiative polariton decay, and affects, therefore, their photoluminescence. Note that our model is only accurate for a low pumping intensity, wherein the population of each polariton state is much less than unity and we can safely neglect exciton-exciton scattering and bosonic stimulated scattering, which is expected to become significant at high pumping intensities.[40,41] Therefore, our equations are linear in the polariton density and all results can be simply rescaled by varying the pump strength.

II. J-AGGREGATE FILMS

Supersaturated solutions of certain organic dyes show a metastable phase in which aggregate formation is evidenced. The organization of aggregates in solution can be fixed by rapid cooling or rapid solvent evaporation. A J aggregate can be typically regarded as a rodlike chain of monomers linked by electrostatic interactions, although different geometries had been proposed and studied in the past years.[32] The dye monomer contains a chromophore responsible for the light-matter interaction in the spectral zone of interest. The aggregates show dramatic changes occurring in the absorption spectra upon supramolecular organization. The aggregate absorption bands are shifted to lower energies by several tens of meV with respect to the monomer transitions and are much narrower. This fact is the signature of the delocalization of excitations along the molecular aggregate with the formation of Frenkel excitons. Exciton delocalization in low dimensional structures leads to super-radiance phenomena, that is, the concentration of the oscillator strength on "in-phase" delocalized exciton states.[32] The high oscillator strength leads to increased light-matter interaction and, therefore, to intense and narrow absorption features and smaller radiative times. It had been evidenced[37–39] that the J-aggregate optical properties can be modeled as a multichromophore system in which both static disorder and thermal exciton decoherence play an important role. For more details about the model applied through this section, we refer to the original references.[37–39] Here, a specific formulation particularly suited for the description of J aggregates used in microcavities will be described. In particular, from our simulations of the J-aggregate film photophysics, the material parameters to be also used in our model of strongly coupled MCs will be determined.

We consider a chain composed of a number of monomers N_d (dyes number) described by the following Frenkel exciton Hamiltonian:

$$H = \sum_{i}^{N_d} E_i b_i^\dagger b_i + \sum_{i \neq j}^{N_d} V_{i,j}(b_i^\dagger b_j + b_j^\dagger b_i). \tag{1}$$

The b_i are the monomer exciton operator, and $E_i = \varepsilon_i + D_i^{\mathrm{agg}}$ is the sum of the bare energy of the monomer excited state and energy shift due to the interaction of the ith excited molecule with the other molecules and the host medium in their ground states. Each dye molecular resonance can be treated as an electrical dipole that causes both couplings with light and with other molecules. When the molecules are put together, the interactions among them give rise to excitation transfer with the formation of delocalized Frenkel excitons and thus to the super-radiance phenomena. We consider a dipolar coupling among the dyes with equal and parallel transition dipole moments. The hopping term is given by $V_{i,j} = -J/|i-j|^3$, where $J > 0$ is the nearest neighbor coupling strength. On the other hand, the presence of diagonal disorder is introduced as a Gaussian stochastic fluctuation of the monomer excitation energies; it leads to the fragmentation of the excitons in localized structures on the aggregate chain, especially at the bottom of the exciton dispersion curve, causing an inhomogeneous broadening. The diagonal disor-

der standard deviation σ is used as the disorder strength parameter. The eigenstates are found by direct diagonalization of the Frenkel exciton Hamiltonian and are described by the following operators:

$$B_\alpha^\dagger = \sum_i c_i^{(\alpha)} b_i^\dagger, \tag{2}$$

where c_i^α is the coefficient of the αth exciton on the ith molecule. The oscillator strength of each state is proportional to

$$F_\alpha = |\sum_i c_i^{(\alpha)}|^2, \tag{3}$$

with $\Sigma_\alpha F_\alpha = N_d$, with molecules of equal dipole transition and with wavelength much greater than the aggregate dimension. Static disorder gives rise to a low energy tail in the exciton density of states, corresponding to partially localized eigenstates. This tail of localized states is of particular interest for optical properties because its states carry almost the whole aggregate oscillator strength and are responsible for the film luminescence and the strong light-matter coupling in MCs.

We describe the dynamics of our system within the framework of a rate equation, including the scattering rates due to a weak linear exciton-phonon coupling, with strength ξ_ω. The "phonons" are a continuous spectrum of molecular vibrations [described by the operators $v_i(\omega)$] located on each chain site with a density of states ρ_ω. The exciton-phonon Hamiltonian is given by

$$H_{\text{ex-}v} = \int \xi_\omega \rho_\omega \sum_i^{N_d} b_i^\dagger b_i [v_i^\dagger(\omega) + v_i(\omega)] d\omega. \tag{4}$$

This choice follows literature reports[37–39] on J-aggregate simulations in neglecting phenomena of stronger phonon-exciton coupling such as the self-trapping mechanism, which, although relevant in some kind of molecular aggregates,[36] are supposed to be not very effective in most cyanine dye J aggregates as suggested by the small value of the Stokes shifts. The phonon-exciton interaction is supposed to be weak so that it can be perturbatively treated as a relaxation mechanism among different exciton states; in other words, molecular vibrations act as a thermal bath for the excitonic system and they do not mix with excitons. All these assumptions are consistent with the fact that emission and absorption experimental features are almost the same and the small differences can be explained as due to exciton relaxation along the dispersion branch and local structures.[38]

The scattering rates calculated in the framework of the Fermi golden rule (see Appendix A for details) are

$$W_{\alpha,\alpha'} = W_0 I_{\alpha,\alpha'} (N_{|\Delta E|} + \Theta_{(\Delta E)}) \left(\frac{|\Delta E|}{J} \right)^p, \tag{5}$$

with

$$I_{\alpha,\alpha'} = \sum_i |c_i^\alpha c_i^{\alpha'}|^2 \tag{6}$$

and making the following assumption:

$$\int \xi_\omega^2 \rho_\omega \delta(\Delta E - \omega) d\omega = \frac{\xi^2}{J} \left(\frac{|\Delta E|}{J} \right)^p. \tag{7}$$

Here, $\Delta E = E_{\alpha'} - E_\alpha$, Θ is the step function, N_E is the Bose–Einstein occupation factor of the states of the vibrational bath, $W_0 = 2\pi\xi^2/(J\hbar)$, and ξ and p are parameters that describe the strength and spectral shape of the exciton scattering with vibrations.[37–39] We also consider the homogeneous linewidth of the states by calculating the broadening of the states due to the radiative lifetime and to the temperature dependent dephasing processes that are dominated by the exciton-phonon scattering. Each exciton state is broadened as a Lorentzian line shape around the bare energy E_α:

$$g_\alpha(E) = \frac{\Delta E_\alpha / \pi}{(E_\alpha - E)^2 + (\Delta E_\alpha)^2}, \tag{8}$$

with the energy uncertainty given by

$$\Delta E_\alpha = \hbar (\sum_{\alpha'} W_{\alpha',\alpha} + \gamma_\alpha). \tag{9}$$

The rate equation for the excitonic system in the low excitation density approximation can be written as

$$\dot{n}_\alpha = \sum_{\alpha'} (W_{\alpha,\alpha'} n_{\alpha'} - W_{\alpha',\alpha} n_\alpha) - \gamma_\alpha n_\alpha + P_\alpha, \tag{10}$$

where we have added the radiative decay rate γ_α, which, for J-aggregate excitons, is given by $\gamma_\alpha = F_\alpha \gamma_0$, where γ_0 is the spontaneous emission of the dye monomer, which is typically $(3\ \text{ns})^{-1}$. We also add a constant pump term P_α on the upper energy tail of the exciton density of states (DOS).

As long as the aggregates are sufficiently diluted, we can calculate the film optical features by summing over an ensemble of independent J aggregates with different disorder configurations. The film absorption is simply the density of states weighted by their oscillator strength; therefore, it is proportional to

$$A(E) = \langle \sum_\alpha F_\alpha g_\alpha(E) \rangle. \tag{11}$$

Photoluminescence should include the population of the exciton levels:

$$PL(E) = \langle \sum_\alpha n_\alpha F_\alpha g_\alpha(E) \rangle. \tag{12}$$

The procedure to obtain the optical features for the J-aggregate film is to sum the single aggregate optical features: we have to create each disordered aggregate, collect its eigenstates with a direct diagonalization and, calculate their oscillator strength, the scattering rates, and the thermal broadenings. Then, we solve the rate equation for the aggregate and find the isolated aggregate steady state and, thus, its optical features. Finally, we have to average the aggregate absorption and/or luminescence spectra over many disorder realizations. We apply the model to fit the experimental absorption and luminescence data of one of the J-aggregate film used for organic microcavities by Ceccarelli *et al.*[19] The simulation shows that with increasing temperature, the absorption and luminescence peaks change their shape, becom-

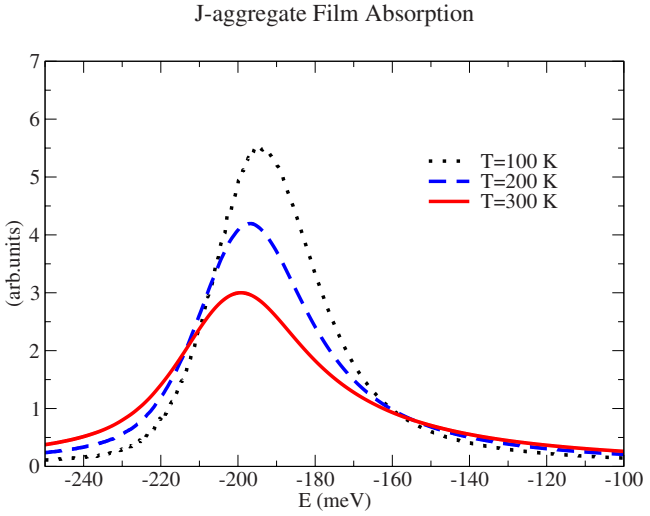

FIG. 1. (Color online) Calculated absorption of a J-aggregate film. With increasing temperatures, the spectrum peak shifts toward the lower energy and is characterized by the asymmetry due to the presence of a high energy tail. Both these two phenomena are accounted for by the differential thermal broadening over the chromophore ensemble.

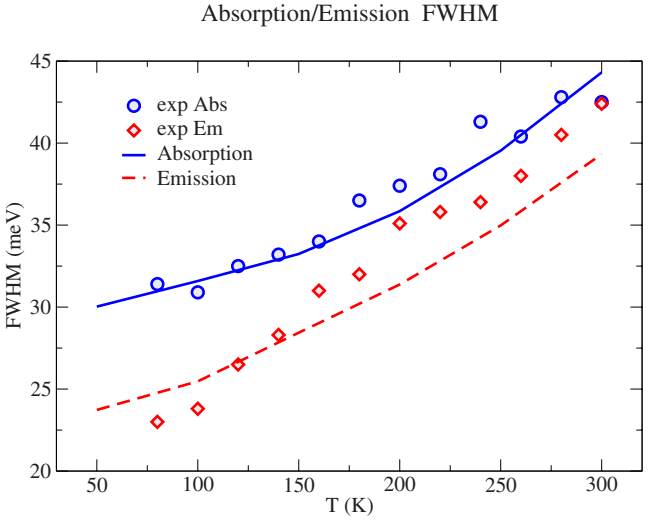

FIG. 2. (Color online) Calculated and experimental absorption and luminescence FWHM with temperature (experimental data from Ref. 19). The FWHM is due to the joint effect of the temperature independent inhomogeneous distribution of excitons and their thermal broadening.

ing more asymmetric, with the peak maximum shifting toward lower energies and the raise of a high energy tail, as can be seen in Fig. 1. This is consistent with the fact that the chromophores feel different thermal broadenings and, in particular, higher energy states suffer greater thermal broadening, being nearer to the delocalized excitations in the J band. We should remark that experimental peak shifts are typically stronger and include the contribution of further effects not considered here such as thermal structural deformations or the real part of the exciton-phonon self-energy.[39] The behavior of the absorption and luminescence full width at half maximum (FWHM) as a function of temperature is reproduced well by our simulations, as shown in Fig. 2.

Here, the following parameter values have been used: $J=75$ meV, $\sigma=0.54$ J, $p=0.8$, $W_0=3.2$ J/$\hbar$, and they will also be used in Sec. III. The ensemble average is done over 50 000 aggregates with length $N_d=100$. The choice of N_d has been guided by the fact that the aggregate physical size should be longer than the coherence length induced by static disorder.

III. J-AGGREGATE ORGANIC MICROCAVITIES

J-aggregate films in a strongly coupled microcavity show a new kind of quasiparticle, which is the cavity polaritons, due to the interaction among Frenkel exciton and confined photon modes. The cavity polaritons are mixed Frenkel exciton-photon states with a dispersion characterized by an anticrossing among lower and upper branches with energy separation Δ called the Rabi splitting. In J-aggregate microcavities, the Frenkel excitons are localized on each aggregate and it is only the interaction with light that induces the polariton coherence over the whole film. In the realistic disordered J-aggregate film, some inhomogeneity is present due to the random positions and orientations of the aggregates and to the energy fluctuation of the super-radiant states (diagonal disorder) distributed around the film absorption peak. In spite of the landscape inhomogeneity, the polariton nature remains delocalized in the "coherent" zones,[23] while some degree of localization is expected outside the coherent end points.

Here, we do not deal with polariton localization, but we focus on the coherent regions, considering the strong coupling zone to be limited by wave vectors below $q_{\max}$, while the rest of the Brillouin zone remains uncoupled. It is well known[23,25–27] that at the bottom of the polariton branches and for large wave vectors of the LP branch, the states are localized incoherent excitations. For the detuning values considered here, the incoherent states above $q_{\max}$ along the LP branch can be considered as uncoupled Frenkel excitons, as in a film with no cavity. Such states include the vast majority of available states and are considered here as the ER states. Given R, which is the average distance between different aggregates in the film [about 200 Å (Ref. 22)], the ratio between polariton states and uncoupled exciton states is $\frac{R^2 q_{\max}^2}{N_d}$, which is of the order of 10^{-3}. The partially localized states at the bottom of the polariton branches, and especially those at the bottom of the LP branch, have a smaller density of states and, in general, a significant photon component; they can be considered as localized polaritons. We can, however, disregard the localized nature of the latter while considering the excitation dynamics because the polariton to polariton phonon mediated scattering is significantly slower than polariton radiative decay, while the exciton reservoir states to polariton scattering rates do not depend on the localized or extended character of the polaritons. In fact, if we consider a polariton localized on a number n_{loc} of aggregates, the ER to polariton scattering is obtained by summing all the processes leading from the excitons on any one of the n_{loc} aggregates to the polariton state. The number of such processes is proportional to n_{loc}, but, on the other hand, the probability of each of them is proportional to the polariton

weight on one aggregate, which scales as $1/n_{\mathrm{loc}}$; the net result is that the total ER to polariton scattering rate is on average independent of the polariton localization degree. In order to set up a model delocalized wave function for the polariton states, we proceed then as follows.

It has been shown[25] that in the coherent regions of the polaritonic dispersion, the states are ideal-polariton-like: with a plane wave character, well defined wave vector, uniformly extended over the whole cavity. A coherent polariton of wave vector k can be thought of as the superposition of the k photon mode plus a delocalized exciton part contributed by the exciton states of the film J aggregates. We write a delocalized upper polariton operator as

$$p_{k,U}^{+} = C_{k,U}^{(\mathrm{ph})} c_k^{+} + \frac{C_{k,U}^{(\mathrm{ex})}}{\sqrt{N_{\mathrm{agg}}}} \sum_{I}^{N_{\mathrm{agg}}} \sum_{\alpha}^{N_d} \phi_{\alpha,I}^{(k)} B_{\alpha,I}^{+}, \tag{13}$$

with a similar expression for the lower polariton, where c_k is the operator for the confined photon[42] and, as for ideal polaritons, $C_k^{(\mathrm{ex})}$, $C_k^{(\mathrm{ph})}$ are the usual Hopfield coefficients corresponding to the two coupled oscillator model. The exciton coefficients $\phi_{\alpha,I}^{(k)}$ describing how each exciton α of each aggregate I participates in the polariton states do not depend on the polariton branch index (upper or lower) and are modeled as follows. The ideal-like polaritons are extended with equal degree on each one of the N_{agg} aggregates and we make the assumption that the weight in the polariton states of each exciton is proportional to its oscillator strength. We stress that the phases of $\phi_{\alpha,I}^{(k)}$ in our model wave function are immaterial for our simulations because only the exciton weight in each polariton matters in the calculations of the scattering rates induced by on site molecular vibrations via the Fermi golden rule (see Appendix A). We thus get $|\phi_{\alpha,I}^{(k)}| = \sqrt{F_\alpha / N_d}$, which are the relevant quantities entering the scattering rates and do not depend on the polariton branch index (upper or lower) nor on the polariton wave vector.

The polariton dispersion curve given by the usual two coupled oscillator model is

$$E_{U,L}(k) = \frac{1}{2}[E_0 + \epsilon_k \pm \sqrt{(E_0 - \epsilon_k)^2 + \Delta^2}], \tag{14}$$

with E_0 being the mean energy of the super-radiant excitons, corresponding to the absorption maximum at the bottom of the J band, while $\epsilon_k = \frac{\hbar c}{n_r}(k_0^2 + k^2)^{1/2}$ is the first photon mode dispersion curve, with k_0, n_r being the MC vertical quantization wave vector and the effective refractive index. Figure 3 shows the polariton dispersion curve together with the DOS of the excitonic reservoir formed by the J-aggregate excitons.

The excitonic part of the system is still affected by the exciton-phonon interaction and thus relaxation in the strongly coupled system is introduced by this mechanism. Besides the delocalized polariton states, there are a number of uncoupled exciton states on each J aggregate (the ER states). The scattering processes take place from the initial to the final state excitonic components of the different quasiparticles, thus among molecular excitons within an aggregate, and also between a pure exciton and the exciton component of a polariton or between an exciton component of a polariton and that of another polariton. In order to simulate the

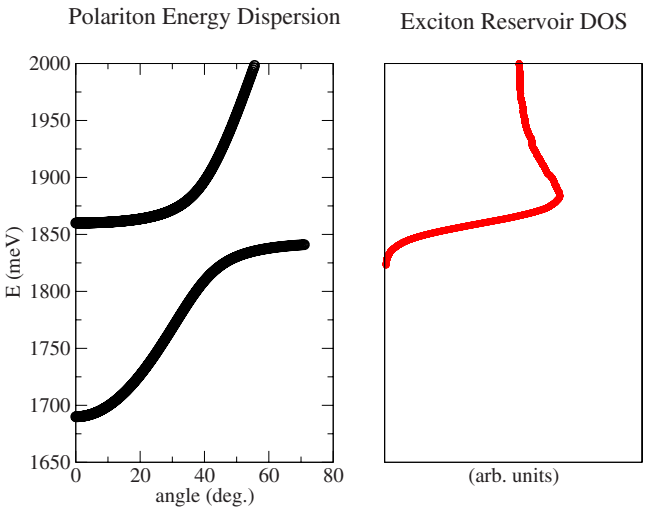

FIG. 3. (Color online) Polariton dispersion curve and DOS of J-aggregate reservoir excitons. The Rabi splitting is 80 meV, with a detuning $(E_0 - \epsilon_0)$ of 150 meV.

dynamics in the rate equation approach, we should calculate all possible scattering rates. Note that considering localized vibrations, the scattering promotes the relaxation among states that have a common exciton participation on the same site of the same aggregate. The calculation of the different scattering rates via the Fermi golden rule, as for the J-aggregate film, is detailed in Appendix A. The scattering rate from an exciton, $n' = (\alpha, I)$, which is the αth exciton of the Ith aggregate, to a polariton k is given by

$$W_{k,n'} = W_0 \frac{D(k)|C_k^{(\mathrm{ex})}|^2}{N_{\mathrm{agg}}} I_{n'}^{(\mathrm{ex\text{-}pol})} (N_{|\Delta E|} + \Theta_{(\Delta E)}) \left(\frac{|\Delta E|}{J} \right)^p, \tag{15}$$

where $I_{n'}^{\mathrm{ex\text{-}pol}}$ is an overlap factor between the exciton and the polariton, $\Delta E = E_k - E_{n'}$, and $D(k)$ is the number of states corresponding, in our inverse space grid, to the polariton variable of modulus wave vector k. For the opposite processes, we get

$$W_{n',k} = W_0 \frac{|C_k^{(\mathrm{ex})}|^2}{N_{\mathrm{agg}}} I_{n'}^{(\mathrm{ex\text{-}pol})} (N_{|\Delta E|} + \Theta_{(\Delta E)}) \left(\frac{|\Delta E|}{J} \right)^p, \tag{16}$$

where $\Delta E = E_{n'} - E_k$. The scattering rate between polaritons is given by

$$W_{k',k} = W_0 \frac{D(k')|C_{k'}^{(\mathrm{ex})}|^2 |C_k^{(\mathrm{ex})}|^2}{N_{\mathrm{agg}}^2} I^{(p\text{-}p)} (N_{|\Delta E|} + \Theta_{(\Delta E)}) \left(\frac{|\Delta E|}{J} \right)^p, \tag{17}$$

where $I^{(p\text{-}p)}$ is an excitonic overlap factor between polaritons and $\Delta E = E_{k'} - E_k$.

In addition to the phonon mediated scattering, we have also considered a radiative pumping rate from exciton to polariton in the following form:

$$W_{k,\alpha}^{\mathrm{rad}} = \beta^{\mathrm{rad}} \gamma_\alpha \frac{D(k)|C_k^{(\mathrm{ph})}|^2 g_\alpha(E_k)}{\sum_{k'} D(k')|C_{k'}^{(\mathrm{ph})}|^2 g_\alpha(E_{k'})}, \quad (18)$$

such that its contribution is proportional to the exciton oscillator strength and the transfer should match energy conservation, while the normalization is chosen to obtain a net exciton radiative decay toward polaritons of β^{rad} times the spontaneous emission (γ_α). The broadening g_α is given by Eq. (8), wherein the broadenings are calculated for the new cavity system.

To deal with the 2D microcavity, we assume isotropic conditions in which the polariton population depends only on the modulus of the wave vector. Experimentally, this situation can be orthogonally imposed by pumping to the surface of the microcavity or can happen due to fast elastic scattering processes. We describe the dynamics of excitation relaxation by means of a rate equation for the population of state $f_i(t)$:

$$\dot{f}_i(t) = -\Gamma_i f_i(t) + \sum_{i'} [W_{i,i'} f_{i'}(t) - W_{i',i} f_i(t)] + P_i, \quad (19)$$

where the indices i, i' run over all the spectrum of excitations and can refer to both polariton (k, upper or lower) or localized excitons (n). The damping rate due to the escape through the cavity mirrors is given by $\Gamma_i = \frac{|C_i^{(\mathrm{ph})}|^2}{\tau}$. The typical photon lifetime is about $\tau = 35$ fs, corresponding to a photon linewidth of the order of 30 meV. P is the pumping rate that we apply as for the aggregate film to the high energy tail of the J band. For the upper and lower polaritons, we consider the reciprocal space up to the wave vectors $k < 88\,000\ \mathrm{cm}^{-1}$ discretized in a grid of 280 points associated with the modulus of the wave vector. The reservoir is formed by averaging over an ensemble of 1000 J aggregates each with $N_d = 100$ monomers. This means that our simulation actually includes the excitons coming from only 1000 independent disordered aggregates instead of the N_{agg} of the film. This is taken into account by rescaling the polariton to exciton scattering rates in the rate equation by a factor of $N_{\mathrm{agg}}/1000$.

Given the large number of states involved and the fact that two different time scales are present (a fast one related to the intra-aggregate relaxation and a slow one related to the exciton reservoir to polariton relaxation), the direct solution of the rate equation is not numerically feasible. However, by exploiting the difference between the two time scales involved, we can accurately calculate the steady state polariton population under continuous nonresonant pumping with a two-step approach, which has been checked by comparing it to a full direct solution for the case of a single disorder configuration (i.e., $N_{\mathrm{agg}} = 1$). As the exciton to polariton scattering rates are much slower than the polariton radiative decay, the polariton population remains a tiny fraction[43] of the total population and we can safely neglect the effect of particle redistribution from the polariton branches to the exciton states of the ER on the equilibration of the ER itself. In the first step, we thus calculate the steady state J-band population for an ensemble of aggregates, as determined by the high energy pumping and the nonradiative and radiative exciton to polariton scattering rates (neglecting at this stage any polariton to ER backscattering). From the calculated ER population, we obtain then the exciton to polariton pumping rates, which are the number of particles that scatter from the ER to each of the polariton states in the unit time. With the ER in stationary conditions and disregarding other channels for the decay of the uncoupled excitons,[44] the total value of the polariton pumping is, of course, equal to the high energy nonresonant pumping of the ER.[45] In the second step of the calculation, we are restricted to the polariton system alone and we can find the polariton steady state resulting from the interplay of exciton to polariton pumping, photon escape through the mirrors, polariton scattering back into the exciton reservoir, and intra- and interbranch polariton scatterings.

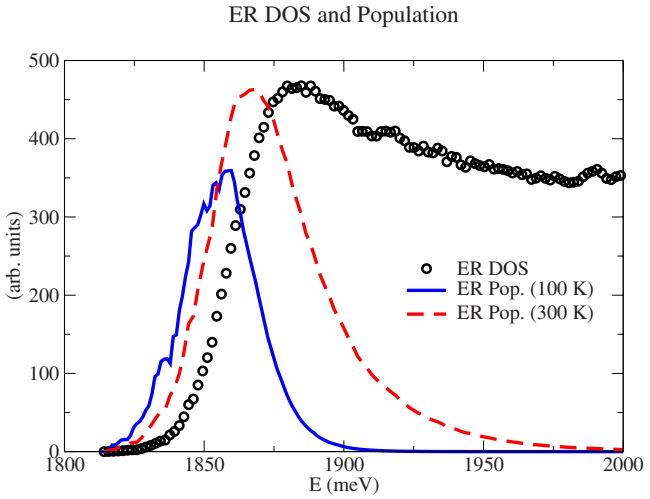

FIG. 4. (Color online) Excitonic reservoir density of states (circles) and exciton reservoir steady state population for $T = 100$ K and $T = 300$ K (full and segmented line, respectively). At $T = 100$ K, the population distribution reflects the inhomogeneous and disconnected nature of the exciton reservoir, while at $T = 300$ K, the population distribution is smoother.

We now discuss the scattering rates and the ER population calculated with our model for a system with a Rabi splitting of 80 meV and a detuning of 150 meV, as shown in Fig. 3. The calculations were performed by using the same set of parameters employed for the bare film simulations in Sec. II.

The exciton reservoir DOS, which can be seen in Fig. 4, has a disconnected nature because it is the sum of individual aggregates. The relaxation inside each aggregate is fast with respect to the exciton decay into polaritons, and thus, the population of each aggregate is very close to its thermal equilibrium value. The ER population distribution is the sum of those of the individual aggregates in the ensemble. At low temperatures, the ER population distribution reflects the inhomogeneous distribution of the bottom states of the aggregates. For $T = 300$ K, the population distribution is smoother and almost identical to a thermally populated ER DOS.

On the other hand, the polariton lifetime finiteness effectively competes with the nonradiative scattering processes and limits the polariton thermalization. In fact, the polariton radiative escape is the fastest rate acting on the polariton branches (Fig. 5).[46] The polariton to ER decay is also important for the UP branch and becomes more relevant at higher temperatures. The mean polariton pumping rate from an ex-

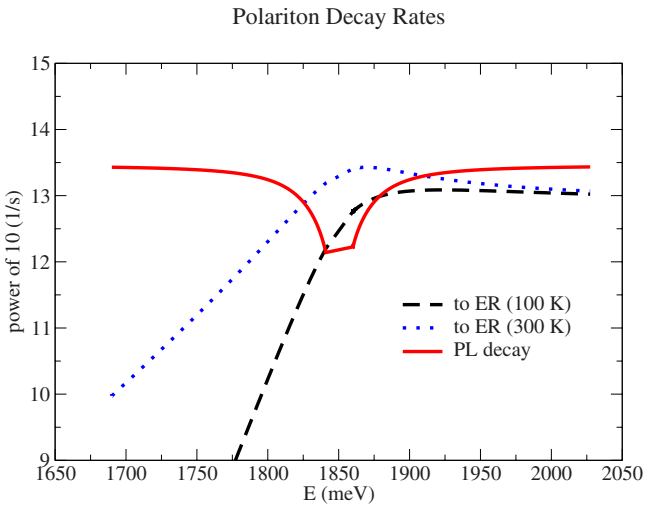

FIG. 5. (Color online) The polariton radiative decay (full line) and the polariton to ER scattering rate at $T=100$ K (segmented line) and $T=300$ K (dotted line) as a function of energy.

citation in the reservoir is also shown in Fig. 6.[46] The calculation of the rates shows that the relaxation intra- and interpolariton branches is strongly suppressed by the polariton depletion due to the small photon time of escape in J-aggregate microcavities (about 35 fs). The dynamics of the J aggregate is significantly faster with respect to the nonradiative transfer rate from exciton to polariton, which is plotted in Fig. 6, so that the reservoir results to be in good approximation at thermal equilibrium while the exciton to polariton pumping takes place, which justifies the two-step numerical procedure to solve the rate equation [Eq. (19)]. We can observe that at $T=300$ K, the pumping rate for the UP branch is increased by almost an order of magnitude with respect to $T=100$ K. This fact is responsible for the activation behavior of the UP photoluminescence intensity. At $T=300$ K, the nonradiative decay of the polaritons to the ER

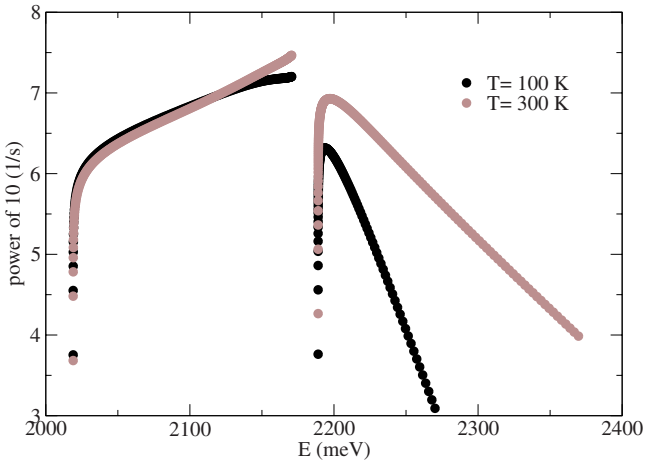

FIG. 6. (Color online) The mean value of the exciton to polariton pumping rate as a function of polariton energy for $T=100$ K and $T=300$ K. Such value is averaged on the exciton reservoir population.

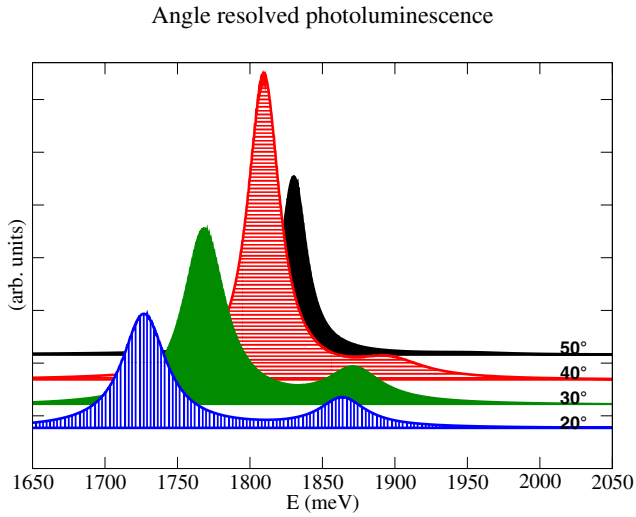

FIG. 7. (Color online) Angle-resolved photoluminescence for a cavity with a Rabi splitting of 80 meV at 300 K, which is calculated for angles of 20°, 30°, 40°, and 50°.

is also important, particularly for high Rabi splitting values. The signature of its effectiveness on the upper branch is in the greater broadening of the UP lines with respect to that of the lower polaritons. Although we employed a continuous spectrum of vibrations instead of a set of definite vibrational quanta, the rates calculated herein are in qualitative agreement with the estimation given in Refs. 23, 30, and 31. The UP nonradiative decay time into the ER is about tens of femtoseconds while in Refs. 23 and 31, the estimation is 20 fs. The nonradiative decay time of an incoherent exciton to the LP polariton states is about 350 ps for $\Delta=80$ meV, following the calculation in Refs. 30 and 31. In our model, such time is of the order of hundreds of picoseconds, as can be extracted from the exciton to polariton scattering rates of Fig. 6.

From the polariton population, we are able to construct the angle-resolved cw photoluminescence, imposing the in-plane wave vector and energy match between polaritons and external photons. We also need to consider the polariton energy broadening of the same kind as in Eq. (8) and a wave vector uncertainty due to the wave vector representation given by our numerical grid. The polariton angle-resolved photoluminescence calculated by our model is shown in Fig. 7 for a MC with a Rabi splitting of 80 meV. The major contribution is from the lower polariton branch except for very small angles, which are not shown here. Focusing on the resonant angle of 39°, which is the angle under which the energy of the photon cavity mode is equal to the exciton resonance, we can observe (Fig. 8) that the upper polariton contribution is about a hundred times less intense at low temperature. By increasing the temperature of the vibrational bath, the nonradiative scattering processes are enhanced and thermally activated (see Figs. 5 and 6). In addition, the almost thermalized ER population at higher temperature occupies higher energy states, as observed in Fig. 4 near the UP branch. As already mentioned, the typical parameter used to analyze the dynamics of organic MCs is the ratio between the UP and the LP luminescence: $C=\frac{\mathcal{L}_{\mathrm{UP}}}{\mathcal{L}_{\mathrm{LP}}}$ at the anticrossing

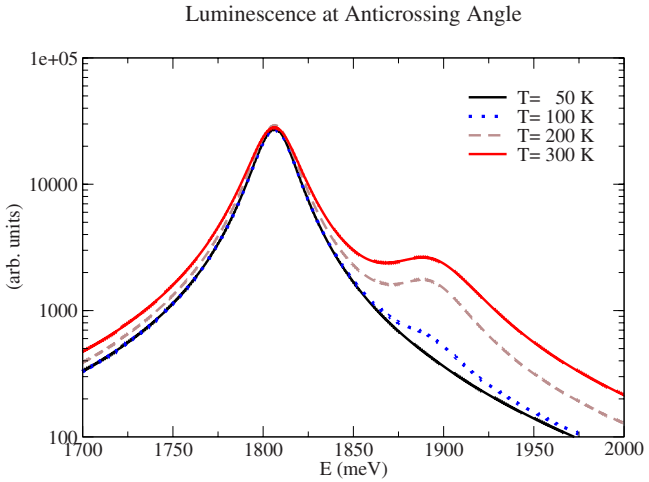

FIG. 8. (Color online) Calculated luminescence following nonresonant pumping for a J-aggregate microcavity with a Rabi splitting of 80 meV at resonance angle (39°). The upper polariton contribution exhibits an activation with increasing temperature.

angle, wherein the photonic components are equal for the lower and upper polaritons. Such ratio is calculated by fitting the corresponding photoluminescence spectra (Fig. 8) with two Lorentzian shapes in order to distinguish the contribution of the upper and lower polariton branches. The C index is given then by the amplitude ratio of the upper and lower Lorentzian shapes. The upper polariton experimental luminescence exhibits a thermal activation (Fig. 9). This fact can be reproduced by our model by neglecting the radiative transfer process of Eq. (18) ($b^{\mathrm{rad}} \simeq 0$). When included, the radiative transfer process leads to an almost equal pumping of LP and UP polariton states from the ER; this process is almost temperature independent and is responsible for a low temperature UP photoluminescence. Increasing the strength of such process leads to the increase in a photoluminescence

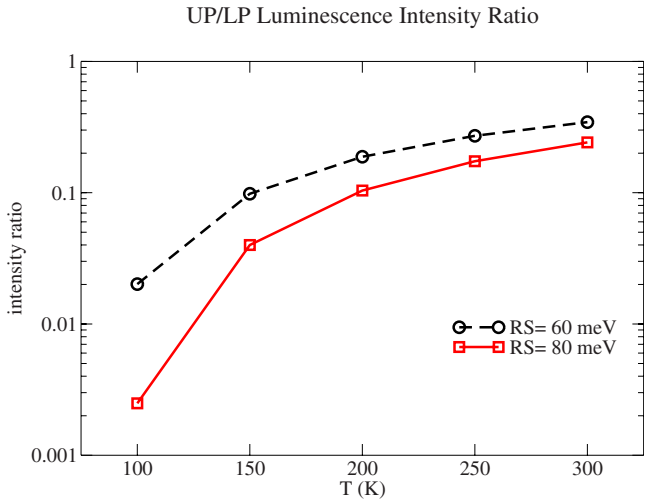

FIG. 9. (Color online) UP/LP luminescence ratio at resonance angle for a system with Rabi splittings of 60 and 80 meV. The intensity ratio exhibits a thermal activation of UP population due to the activation of the exciton reservoir to upper polariton phonon mediated scattering.

base line, on top of which appears the thermal activation contribution due to scattering with phonons at high temperatures, which can explain the finite low temperature UP/LP luminescence ratio in Ref. 29. If the efficiency β^{rad} of such pumping process is sufficiently strong, it becomes dominant with respect to the phonon scattering processes considered here and the thermal activation is not observable any more within our model.

In Fig. 9, the luminescence intensity ratio C is shown for microcavities with Rabi splittings of 60 and 80 meV, without the radiative process. With increasing temperature, we found that the UP contribution displays a thermal activation that is due to the activation of the scattering rates that lead from the excitonic reservoir to the upper polariton states. The calculated intensity ratio C in the temperature range between 100 and 300 K can be easily fitted as an Arrhenius-like behavior with activation energies of about 28 and 42 meV for MCs with Rabi splitting values of 60 and 80 meV, respectively. As we have employed a continuous of vibrational mode, the values of the activation energies are not related to a specific vibration but rather reflect the energy distance between the UP branch and the bottom of the J band; in fact, the activation energies are very near to half of the Rabi splitting value. In Appendix B, we present a schematic analytical model that explains this behavior. Such photoluminescence results are in qualitative agreement with the activation behavior reported in the experimental data.[19,29]

In conclusion, a theory of the photoexcitation dynamics of strongly coupled J-aggregate MCs that accounts for all the different accessible excitations of the system and includes scattering with a thermal bath of localized vibrations with a continuous spectrum yields qualitative agreement with experimental photoluminescence data. The use of a model polariton wave function for the disordered MC allows to directly relate its optical properties to those of J-aggregate film. The numerical simulations explain the UP/LP luminescence intensity ratio under nonresonant cw pumping as a function of temperature. The uncoupled excitons rapidly thermalize in the exciton reservoir and then the pumping of upper polaritons occurs via the absorption of a vibrational quantum from the bottom of the J band and, therefore, suffers thermal activation.

ACKNOWLEDGMENTS

We wish to thank V. M. Agranovich and D. G. Lidzey for many useful discussions. Partial financial support from MIUR (Grant No. PRIN 2006-021037) and from the European Commission via the 5th Framework research training network "HYTEC" (Contract No. HPRN-CT-2002-00315) is gratefully acknowledged.

APPENDIX A: SCATTERING RATE DERIVATION

The scattering rates with emission and/or absorption of a vibrational mode are calculated in the framework of the Fermi golden rule, starting from the following exciton-phonon linear Hamiltonian:

$$H_{\text{ex-}v} = \int \xi_\omega \rho_\omega \sum_{I,i}^{N_{\text{agg}},N_d} b_i^\dagger b_i [v_i^\dagger(\omega) + v_i(\omega)] d\omega. \quad \text{(A1)}$$

ξ_ω is the coupling parameter, ρ_ω is the vibrational density of states, and the local vibrations are associated with each dye site of each one of the aggregates.

Let us show how the calculation of the total scattering rate $W_{\alpha',\alpha}$, which is from two excitons inside the same aggregate $\alpha \to \alpha'$, is performed. We need to sum all the different scattering processes involving localized vibrations in the aggregate that lead from α to α'. For example, the process that involves one vibration of energy ω in the site i has a rate given by

$$\frac{2\pi}{\hbar} |\xi_\omega c_i^{(\alpha)*} c_i^{(\alpha')}|^2 [\delta_{(E_{\alpha'}-E_\alpha-\hbar\omega)} n_\omega + \delta_{(E_{\alpha'}-E_\alpha+\hbar\omega)}(n_\omega+1)], \quad \text{(A2)}$$

where we have written both the scatterings for the absorption and the emission of the local vibration. The term between squared brackets, which will be indicated by $\mathcal{T}(\omega)$, contains the Dirac deltas selecting the local vibration of the correct energy $\Delta E = E_{\alpha'} - E_\alpha$ corresponding to the energy separation between the two exciton states. If $\Delta E > 0$, the scattering is proportional to $n_{|\Delta E|}$ because it happens with an absorption of a local vibration proportional to their availability, and so of their number; otherwise, the process involves the emission of a phonon and is proportional to $(n_{|\Delta E|}+1)$. The factor $\mathcal{T}(\omega)$ depends only on the energy of α and α' and does not depend on the site in which the local vibration is interacting with the exciton. For this reason, we can take such term outside the summation over the different processes, involving vibrations on all the monomer sites of a J aggregate. The total scattering rate is therefore

$$\frac{2\pi}{\hbar} \int \mathcal{T}(\omega) \xi_\omega^2 \rho_\omega d\omega I_{\alpha,\alpha'}, \quad \text{(A3)}$$

where the exciton overlap factor is

$$I_{\alpha,\alpha'} = \sum_i |c_i^\alpha c_i^{\alpha'}|^2. \quad \text{(A4)}$$

Such overlap factor means that the scattering takes place only if two excitons have amplitude on the same position of the aggregate chain. This also remains true for the polariton scattering rates and is due to the localized nature of the vibrations. The integration in ω selects the local vibration of energy ΔE. We assumed for the following function a simple power law:

$$\frac{2\pi}{\hbar} \xi_{|\Delta E|}^2 \rho_{|\Delta E|} \equiv W_0 \left(\frac{|\Delta E|}{J} \right)^p. \quad \text{(A5)}$$

The total scattering rate is therefore given by

$$W_{\alpha,\alpha'} = W_0 I_{\alpha,\alpha'} (N_{|\Delta E|} + \Theta_{(\Delta E)}) \left(\frac{|\Delta E|}{J} \right)^p. \quad \text{(A6)}$$

We have chosen a simple power shape for the function in Eq. (A5), following the original model,[37–39] with p chosen to obtain the best fit of the experimental absorption FWHM (Fig. 2). This rather crude model suffices in explaining the temperature dependence of the cavity polariton photoluminescence, while for the actual detailed photoluminescence shape of the J-aggregate MC, a more accurate knowledge of the function in Eq. (A5) is needed. We could expect such function to be composed by a continuum wing at low energies and a series of peaks corresponding to the dye molecular optical vibrations in the host environment.

The scattering rates for the polariton system are calculated in an analogous way. For example, let us calculate the scattering rate from the polariton k to the exciton α in the aggregate I due to the interaction via a vibration of energy ω in the site i of I. The amplitude of the exciton component of the polariton on such site is given by

$$\frac{C_k^{(\text{ex})}}{\sqrt{N_{\text{agg}}}} \Phi_{i,I}^{(k)} = \frac{C_k^{(\text{ex})}}{\sqrt{N_{\text{agg}}}} \sum_{\alpha' \in I} \phi_{\alpha',I}^{(k)} c_i^{\alpha'}.$$

The scattering rate is therefore given by

$$\frac{2\pi}{\hbar} \left| \frac{C_k^{(\text{ex})}}{\sqrt{N_{\text{agg}}}} \xi_\omega \Phi_{i,I}^{(k)*} c_i^\alpha \right|^2 [\delta_{(E_\alpha - E_k - \hbar\omega)} n_\omega + \delta_{(E_\alpha - E_k + \hbar\omega)}(n_\omega + 1)]. \quad \text{(A7)}$$

As before, the term $\mathcal{T}(\omega)$ depends only on the energy difference $\Delta E = E_\alpha - E_k$ and not on the site of the vibration. The total rate also includes a summation on all the dye sites inside the aggregate I and reads

$$\frac{2\pi}{\hbar} \frac{|C_k^{(\text{ex})}|^2}{N_{\text{agg}}} \left(\int \mathcal{T}(\omega) \xi_\omega^2 \rho_\omega d\omega \right) \sum_i^{N_d} |\Phi_{i,I}^{(k)} c_i^\alpha|^2. \quad \text{(A8)}$$

The integration on ω is performed as before and we get

$$W_{\alpha,k} = W_0 \frac{|C_k^{(\text{ex})}|^2}{N_{\text{agg}}} I_{\alpha,I;k} (N_{|\Delta E|} + \Theta_{(\Delta E)}) \left(\frac{|\Delta E|}{J} \right)^p, \quad \text{(A9)}$$

with

$$I_{\alpha,I;k} = \sum_{\beta,\beta' \in I} \phi_{\beta,I}^{(k)} \phi_{\beta',I}^{(k)*} \sum_i^{N_d} |c_i^\alpha|^2 c_i^\beta c_i^{\beta'*}. \quad \text{(A10)}$$

The overlap factor $I_{\alpha,I;k}$ between the polariton k and the exciton α does not depend on the polariton branch index (upper or lower). Furthermore, it does not depend on the phase of the polariton amplitude on the exciton α of the I aggregate ($\phi_{\alpha,I}^{(k)}$) because of the following argument. The molecular aggregate is much shorter than the light wavelength so the light-matter coupling of a photon k with an exciton α in the aggregate I has the phase $e^{i\vec{k}\cdot\vec{r}_I}$. All the excitons inside a given aggregate are approximately coupled with light with the same phase, and therefore, inside the polariton wave function, they acquire the same phase. The phase depends only on the aggregate position, and therefore, it is the same for all the excitons inside the same aggregate. The summation in Eq. (A10) reduces to

$$I_{\alpha,I;k} = \sum_{\beta,\beta' \in I} \frac{\sqrt{F_\beta F_{\beta'}}}{N_d} \sum_i^{N_d} |c_i^\alpha|^2 c_i^\beta c_i^{\beta' *}.$$

It is not dependent on the polariton wave vector k and we can define $I_{\alpha,I}^{(\text{ex-pol})} = I_{\alpha,I;k}$, which corresponds to $I_{n'}^{(\text{ex-pol})}$ with the notation of Eq. (15). The inverse process, $\Delta E = E_k - E_\alpha$, gives a similar result, but we should also multiply for the final number of polariton states corresponding to the free variable k, that is, $D_{U,L}(k)$:

$$W_{k,\alpha} = W_0 \frac{D(k)|C_k^{(\text{ex})}|^2}{N_{\text{agg}}} I_{n'}^{(\text{ex-pol})} [N_{|\Delta E|} + \Theta(\Delta E)] \left(\frac{|\Delta E|}{J} \right)^p, \tag{A11}$$

with the number of the states in the inverse space grid, which is associated with the free variable k that is given with good approximation (only for vanishing wave vector are the significant differences) by

$$D(k) = \frac{2\pi k}{2\pi/L}, \tag{A12}$$

where L is the lateral quantization length.

The polariton to polariton scattering from $k \to k'$, with emission or absorption of a vibration ω in the site i of the aggregate I calculated via the Fermi golden rule, is proportional to the square of the Hamiltonian matrix element:

$$\frac{C_k^{(\text{ex})} C_{k'}^{(\text{ex})}}{N_{\text{agg}}} \xi_\omega \Phi_{i,I}^{(k)*} \Phi_{i,I}^{(k')}.$$

By following the same passages as before, summing over the dye sites and over all the aggregates, we obtain the following scattering rate:

$$W_{k',k} = W_0 \frac{D(k')|C_{k'}^{(\text{ex})}|^2 |C_k^{(\text{ex})}|^2}{N_{\text{agg}}^2} I^{(p\text{-}p)} (N_{|\Delta E|} + \Theta_{(\Delta E)}) \left(\frac{|\Delta E|}{J} \right)^p, \tag{A13}$$

where $\Delta E = E_{k'} - E_k$. The polariton-polariton overlap factor is given by

$$I^{(p\text{-}p)} = \sum_I \sum_{\alpha,\alpha',\beta,\beta'} \phi_{\alpha,I}^{(k)*} \phi_{\alpha',I}^{(k)} \phi_{\beta,I}^{(k')} \phi_{\beta',I}^{(k')*} \sum_i c_i^{\alpha *} c_i^{\alpha'} c_i^\beta c_i^{\beta' *}.$$

The overlap factor, which does not depend on polariton branch indices (upper or lower), for the same argument invoked before is independent of the phases of $\phi_{\beta',I}^{(k)}$ and, thus, does not depend on the k', k polaritons:

$$I^{(p\text{-}p)} = \sum_I \sum_{\alpha,\alpha',\beta,\beta'} \frac{\sqrt{F_{\alpha,I} F_{\alpha',I} F_{\beta,I} F_{\beta',I}}}{N_d^2} \sum_i c_i^{\alpha *} c_i^{\alpha'} c_i^\beta c_i^{\beta' *}.$$

Note that there are N_{agg} different aggregates on which the scattering rates have to be calculated (the sum over I in the previous formula). We simulate such ensemble of aggregates by considering an average of 1000 different aggregate disorder configurations and appropriately rescaling such value by a factor of $N_{\text{agg}}/1000$.

APPENDIX B: THREE-STATE ANALYTICAL MODEL FOR THE UPPER PHOTOLUMINESCENCE/LOWER PHOTOLUMINESCENCE LUMINESCENCE RATIO

The UP thermal activation can be easily explained by introducing an analytical model that takes into account only three states: the ER and UP and LP states at anticrossing. The ER is subjected to a pump term and its population is scattered into the UP and LP anticrossing states. The ER is at a higher energy than the LP branch, so the scattering toward the LP state involves the emission of a phonon; on the other hand, it is at a lower energy with respect to the UP branch, so that the scattering to the UP state requires the absorption of a vibrational quantum. The polariton states do not have time to further scatter because they quickly decay as MC emission. The model rate equations are

$$\dot{N}_{\text{ER}} = P - W_{\text{LP}} N_{\text{ER}} (n_v + 1) - W_{\text{UP}} N_{\text{ER}} n_v,$$

$$\dot{N}_{\text{UP}} = W_{\text{UP}} N_{\text{ER}} n_v - \gamma N_{\text{UP}},$$

$$\dot{N}_{\text{LP}} = W_{\text{LP}} N_{\text{ER}} (n_v + 1) - \gamma N_{\text{LP}},$$

where n_v is the phonon thermal population, γ is the polariton radiative decay rate, and the scattering rates are $W_{\text{LP}} \approx W_{\text{UP}} \approx W$, which is correct if the ER state is energetically equidistant from the UP and LP states. The polariton steady state populations are given by

$$N_{\text{LP}} = \frac{W}{\gamma} N_{\text{ER}} (n_v + 1),$$

$$N_{\text{UP}} = \frac{W}{\gamma} N_{\text{ER}} n_v.$$

The luminescence intensity ratio is thermally activated:

$$C = \frac{\mathcal{L}_{\text{UP}}}{\mathcal{L}_{\text{LP}}} \propto \frac{n_v}{1 + n_v} = e^{-\hbar\omega_v / K_b T}.$$

Such a simple model does not take into account that the ER has a spectral extension and does not take into account the possibility of a radiative decay of excitons into polaritons. These two factors cause the photoluminescence ratio to be finite even at low temperatures, as experimentally seen in Ref. 29.

*michetti@df.unipi.it
†larocca@sns.it

[1] C. Weisbuch, M. Nishioka, A. Ishikawa, and Y. Arakawa, Phys. Rev. Lett. **69**, 3314 (1992).
[2] M. S. Skolnick, T. A. Fisher, and D. M. Whittaker, Semicond. Sci. Technol. **13**, 645 (1998).
[3] G. Khitrova, H. M. Gibbs, F. Jahnke, M. Kira, and S. W. Koch, Rev. Mod. Phys. **71**, 1591 (1999).
[4] A. Kavokin and G. Malpuech, *Cavity Polaritons*, Thin Film and Nanostructures Series Vol. 32 (Elsevier, New York, 2003).
[5] C. Ciuti, P. Schwendimann, and A. Quattropani, Semicond. Sci. Technol. **18**, S279 (2003).
[6] V. Savona, J. Phys.: Condens. Matter **19**, 295208 (2007).
[7] F. Tassone, C. Piermarocchi, V. Savona, A. Quattropani, and P. Schwendimann, Phys. Rev. B **56**, 7554 (1997).
[8] F. Tassone and Y. Yamamoto, Phys. Rev. B **59**, 10830 (1999).
[9] T. D. Doan, H. T. Cao, D. B. Tran Thoai, and H. Haug, Phys. Rev. B **72**, 085301 (2005).
[10] M. Richard, J. Kasprzak, R. Romestain, R. Andr, and Le Si Dang, Phys. Rev. Lett. **94**, 187401 (2005).
[11] J. Kasprzak, M. Richard, S. Kundermann, A. Baas, P. Jeambrun, J. M. J. Keeling, F. M. Marchetti, M. H. Szymanska, R. Andre, J. L. Staehli, V. Savona, P. B. Littlewood, B. Deveaud, and Le Si Dang, Nature (London) **443**, 409 (2006).
[12] D. G. Lidzey, D. D. C. Bradley, M. S. Skolnick, T. Virgili, S. Walker, and D. M. Whittaker, Nature (London) **395**, 53 (1998).
[13] R. J. Holmes and S. R. Forrest, Phys. Rev. Lett. **93**, 186404 (2004).
[14] R. J. Holmes and S. R. Forrest, Phys. Rev. B **71**, 235203 (2005).
[15] D. G. Lidzey, in *Organic Nanostructures: Science and Applications*, International School of Physics Enrico Fermi, edited by V. M. Agranovich and G. C. La Rocca (IOS, Amsterdam, 2002), p. 405.
[16] D. G. Lidzey, in *Electronic Excitations in Organic Based Nanostructures*, Thin Films and Nanostructures Vol. 31, edited by V. M. Agranovich and F. Bassani (Elsevier, San Diego, 2003), Chap. 8.
[17] J. R. Tischler, M. S. Bradley, Q. Zhang, T. Atay, A. Nurmikko, and V. Bulovic, Org. Electron. **8**, 94 (2007).
[18] J. Wenus, S. Ceccarelli, D. G. Lidzey, A. I. Tolmachev, J. L. Slominskii, and J. L. Bricks, Org. Electron. **8**, 120 (2007).
[19] S. Ceccarelli, J. Wenus, M. S. Skolnick, and D. G. Lidzey, Superlattices Microstruct. **41**, 289 (2007).
[20] R. J. Holmes and S. R. Forrest, Org. Electron. **8**, 77 (2007).
[21] V. M. Agranovich, H. Benisty, and C. Weisbuch, Solid State Commun. **102**, 631 (1997).
[22] D. G. Lidzey, D. D. C. Bradley, T. Virgili, A. Armitage, M. S. Skolnick, and S. Walker, Phys. Rev. Lett. **82**, 3316 (1999).
[23] V. M. Agranovich, M. Litinskaia, and D. G. Lidzey, Phys. Rev. B **67**, 085311 (2003).
[24] M. Litinskaya and P. Reineker, Phys. Rev. B **74**, 165320 (2006).
[25] P. Michetti and G. C. La Rocca, Phys. Rev. B **71**, 115320 (2005).
[26] V. M. Agranovich and Y. N. Gartstein, Phys. Rev. B **75**, 075302 (2007).
[27] P. Michetti and G. C. La Rocca, Physica E (Amsterdam) **40**, 1926 (2008).
[28] D. G. Lidzey, A. M. Fox, M. D. Rahn, M. S. Skolnick, V. M. Agranovich, and S. Walker, Phys. Rev. B **65**, 195312 (2002).
[29] P. Schouwink, J. M. Lupton, H. von Berlepsch, L. Dahne, and R. F. Mahrt, Phys. Rev. B **66**, 081203(R) (2002).
[30] M. Litinskaya, P. Reineker, and V. M. Agranovich, J. Lumin. **110**, 364 (2004).
[31] M. Litinskaya, P. Reineker, and V. M. Agranovich, J. Lumin. **119**, 277 (2006).
[32] T. Kobayashi, *J-Aggregates* (World Scientific, Singapore, 1996).
[33] S. de Boer, K. J. Vink, and D. A. Wiersma, Chem. Phys. Lett. **137**, 99 (1987).
[34] H. Fidder, J. Knoester, and D. A. Wierma, Chem. Phys. Lett. **171**, 529 (1990).
[35] I. Renge and U. P. Wild, J. Phys. Chem. A **101**, 7977 (1997).
[36] D. Embriaco, D. B. Balagurov, G. C. La Rocca, and V. M. Agranovich, Phys. Status Solidi C **1**, 1429 (2004).
[37] M. Bednarz, V. A. Malyshev, and J. Knoester, J. Chem. Phys. **117**, 6200 (2002).
[38] M. Bednarz, V. A. Malyshev, and J. Knoester, Phys. Rev. Lett. **91**, 217401 (2003).
[39] D. J. Heijs, V. A. Malyshev, and J. Knoester, Phys. Rev. Lett. **95**, 177402 (2005).
[40] H. Zoubi and G. C. La Rocca, Phys. Rev. B **72**, 125306 (2005).
[41] H. Zoubi, Phys. Rev. B **74**, 045317 (2006).
[42] The cavity photon and the cavity polariton states in an isotropic microcavity should be labeled according to their TE or TM polarization character. After averaging on the randomly oriented J aggregates, however, all scattering rates have only a weak dependence on polarization. Very recent experiments [A. Camposeo, L. Persano, P. Del Carro, T. Virgili, R. Cingolani, and D. Pisignano, Org. Electron. **8**, 114 (2007)] observed a TE-TM splitting of the order of 10 meV in the polariton anticrossing region. As long as such splitting is small compared to the Rabi splitting, the temperature dependence of the unpolarized photoluminescence intensity ratio between UP and LP should not be significantly affected. For these reasons and to reduce the computational burden, here, we are using a scalar model insensitive to the polarization degree of freedom.
[43] From the calculated steady state population, we have that the population ratio between polariton states and exciton reservoir for the system with the dispersion described in Fig. 3 is of the order of $10^{-3}-10^{-4}$ in the temperature range considered.
[44] We take the polariton photoluminescence as the only one channel of decay for the system excitations. We do not take into account the possibility of uncoupled exciton nonradiative decay nor the direct radiative decay of uncoupled excitons into external photons that might be relevant channels of excitation number decay. Their effects, however, would simply be a rescaling of the absolute value of the calculated ER population, leaving unchanged all the polariton optical properties analyzed here.
[45] Here, we are neglecting a direct population of polariton states from high energy nonresonant pumping. In fact, this channel is negligible compared to the one considered here.
[46] Note that the rates plotted in Figs. 5 and 6 show the rate values for each polariton state, which are equally spaced in reciprocal space but not in energy. The rates plotted in Fig. 6 show a steep rise at the bottom of the upper and lower bands due to the increase in the polariton number of states for free variable $D_{U,L}(k)$.